A Model Development of Multi-Component Radiolysis Equilibrium Calculation in Nitrogen-Water System*

Xin Lv,[1] Shu Li,[1,2,3,4] Wentao Zhou,[1] Junlian Yin,[1,†] Qi Luo,[2,3,4] and Dezhong Wang[1]

[1]*School of Nuclear Science and Engineering, Key Laboratory of Nuclear Power Systems and Equipment of Ministry of Education, Shanghai Jiao Tong University, Shanghai 200240, China*
[2]*General Clean Energy Co.,Ltd, Shanghai 200030, China*
[3]*State Key Laboratory S1Nuclear Power Safety Technology and Equipment, China Nuclear Power Engineering Co., Ltd., Shenzhen 518172, China*
[4]*China Nuclear Power Engineering Co., Ltd., Shenzhen 518172, China*

Small modular reactors (SMRs) widely utilize mature pressurized water reactor (PWR) technology. Compared to steam pressurizers, nitrogen pressurizers are more suitable for pressurized water-cooled SMRs due to their compact size and simple structure. However, the use of nitrogen pressurizers introduces challenges, particularly regarding the irradiation effects on nitrogen within the primary cooling system. These effects can alter water chemistry and increase the risk of corrosion. Therefore, it is necessary to analyze the nitrogen decomposition products concentrations for reactor safety. This paper aims to establish a simple calculation model to determine the nitrogen radiolysis product concentration and guide water chemistry control in nitrogen-pressurized reactor systems. From a thermodynamic perspective, the paper employs the radiation chemical yield (g-value) and equilibrium constant method to construct a decomposition calculation model for nitrogen dissolved water under radiation. Across the temperature range of 288 to 473 K, the model exhibits relative deviations from previous experimental data ranging from -25% to 20%. Besides, the study examines how key reactor parameters—such as temperature, nitrogen concentration, and radiation dose rate—affect the equilibrium state, revealing a nonlinear relationship between these conditions and pH. These findings provide orientations for water chemistry management in nitrogen-pressurized reactor systems.

Keywords: Nitrogen pressurizer, irradiation chemical equilibrium , equilibrium constant method, nitrogen compounds, thermodynamics

I. INTRODUCTION

As the greenhouse effect intensifies, reducing carbon dioxide emissions has become a global priority[1]. In contrast to traditional fossil fuel-based power generation, which significantly contributes to greenhouse gas emissions, nuclear energy provides a low-carbon alternative by producing electricity with minimal direct carbon dioxide emissions[2–4]. Consequently, nuclear energy helps mitigating global warming and reducing the environmental impact of energy production [5–8].

In China, the 14th Five-Year Plan for Economic and Social Development, as well as the long-term objectives through 2035, outlined a vision for constructing a clean, low-carbon, safe, and efficient energy system. This plan actively promoted the development of coastal nuclear power, the advancement of small modular reactors (SMRs), and the exploration of offshore floating nuclear power platforms. By 2035, China aims to achieve an operational installed nuclear power capacity of 70 million kilowatts, underscoring the commitment to nuclear energy as a key element of its low-carbon energy strategy.

According to the International Atomic Energy Association (IAEA), small Modular Reactors (SMRs) are defined as nuclear reactors with a power capacity of less than 300 MWe [9]. These reactors offer a variety of advantages, including enhanced cost-effectiveness, reduced carbon emissions, high economic viability, simplified designs, and greater flexibility in site selection [10–12]. Until 2024, there are 68 active SMR designs worldwide, with 22 of them being water-cooled reactors [13]. Notable examples of light water-cooled SMRs include China's ACP100[14, 15], Russia's RITM-200N[16], NuScale[17] and AP300[18] in the United States, CAREM in Argentina[19], SMART in Korea[20], and EDF-NUWARD in France[21]. These diverse designs highlight the innovative potential of SMRs in addressing the evolving energy needs of the global market.

In the case of pressurized water reactors (PWRs), the pressurizer technique plays a crucial role in ensuring reactor safety by maintaining a stable pressure in the primary coolant system[22]. At present, there are three major pressurizer designs: nitrogen gas pressurizer, steam pressurizer and gas-steam pressurizer[23, 24]. Among these, steam pressurizers are the most mature and are widely employed in operational civil PWRs. In contrast, steam-gas pressurizers and gas pressurizer techniques are more commonly employed in experimental and demonstration reactors. For example, NHR-II (Nuclear Heating Reactor-II), REX-10 (Regional Energy Reactor; 10MWth), and SMART (System-Integrated Modular Advanced Reactor) utilized steam-gas pressurizer techniques [23]. However, for SMRs, steam-gas pressurizers and, in particular, gas pressurizers offer advantages such as enhanced maneuverability, a simpler structure, and a more compact volume, making them better candidates[25–27]. In Russia, a nitrogen gas pressurizer has been employed in nuclear icebreak-

* Supported by the National Natural Science Foundation of China:The General Program of National Natural Science Foundation of China (No. 52276158), The Young Scientists Fund of the National Natural Science Foundation of China (No. 52206203) and the Young Elite Scientist Sponsorship Program of the China National Nuclear Corporation(CNNC).

† Corresponding author, jlyin@sjtu.edu.cn

ers like KLT-40s [28]. Nevertheless, despite the potential advantages of steam-gas and gas pressurizers, these technologies remain immature, with many technical details still undisclosed. The successful and widespread adoption of nitrogen gas pressurizers continues to face significant challenges, such as safety, water chemistry control and other operational aspects. Scholars have reported that the nitrogen dissolves into the primary coolant water and reaches a high concentration rapidly[29]. Subsequently, through diffusion and convection, dissolved nitrogen will migrate into the core area. In the core region, nitrogen will be exposed to strong gamma radiation, leading to intricate radiation effects and complex chemistry process[30]. Under irradiation, nitrogen molecules may form into a series of atomic free radicals and excited transient molecules, which can interact with water molecules radiation product like hydroxyl radical, hydrated electron etc.[31]. The complex chemical reactions eventually yield a series of oxy-nitrogen species and hydro-nitrogen compounds such as NH_4^+, NO_2^- and NO_3^- [32–36]. This, in turn, impacts the chemical equilibrium of the primary loop coolant, resulting in alterations to the dissolved hydrogen and oxygen concentration, pH value, conductivity and so on. Besides, there generates some oxidizing radiolytic products like NO_2 , leading to alteration in the corrosion potential. Such changes may potentially elevate the corrosion rate of equipment and lead to the deposition of corrosion products[28, 36].

To improve the application safety of nitrogen pressurizer in SMRs, it is essential to assess the alteration of aqueous chemical parameters through analyses of nitrogen radiolysis compound production. Presently, the radiation-induced decomposition behaviors of pure water have been extensively investigated and its radiation chemistry control in water reactors have been studied[37–41], but the study of solution radiolysis behavior remains inadequate due to its inherent complexity. Some scholars studied the radiation behavior of nitric acid solution and the steel corrosion[42–45], but there is a paucity of studies on the radiolysis of nitrogen-dissolved water, and its decomposition behavior remains unclear. The Ibe team [30, 33, 46, 47] investigated the transient behavior of nitrogen radiolysis in both aqueous solution and steam environments. Their findings suggest that the radiolysis products of nitrogen in a gamma radiation field are influenced by the gas species in the surrounding environment. In aqueous solution, the presence of high O_2 content results in the exclusive formation of NO_3^-. As the H_2 content increases, NH_4^+ gradually becomes the predominant species, with a minor presence of NO_3^- or NO_2^-. In steam environments, the decomposition behavior is similar, but the notable difference lies in the yield of nitrogen radiolysis products. Besides, they proposed a plausible pathway for the transient kinetic reactions of the nitrogen-water system, encompassing 73 reactions of atoms and molecules.

Another study by Dey et al. [48] provided a comprehensive review of the radiolysis behavior of nitrogen and azide compounds in solution. They summarized the intricate relationship between the radiolysis process and various factors, including gas concentration, radiation dose, temperature, and gas-liquid volume ratio. Kabakchi et al. [28] monitored the coolant water chemistry in the primary loop of an icebreaker utilizing nitrogen stabilization. Their findings revealed that the rate of change in ammonia concentration is proportionally related to the cube of the hydrogen concentration. Kim et al. [36]calculated thermodynamic values like free energy changes and redox potentials for various nitrogen radiochemical reactions to predict their stability in PWR conditions. Their results suggested that oxidizing conditions favor NO_3^- and NO_2^- formation and reducing conditions promote NH_4^+ formation. While existing researches have provided a foundational understanding of the nitrogen radiolysis reaction pathway and related parameters, the authentic pathways and some reaction rate constants still remains unknown.

To calculate the yield of nitrogen radiolysis compounds, one prevailing model is based on the reaction kinetic method (as indicated by Eq. 1) at which specific elementary reactions and their reaction rate constants are essential[43]. Numerous scholars have utilized the reaction kinetics method to predict the yield of water radiolysis products under diverse reactor conditions [49]. Li et al. conducted a calculation of coolant radiolysis products in operating conditions during the shutdown of PWRs without nitrogen[50]. They suggest that lots factors include temperature, initial material concentrations will influence the radiation products yield and they find that H_2O_2 and O_2 are mutually promoted, which can be inhibited to some extent by adding H_2. Regarding the nitrogen-water system, Ibe et al. established a computational model by the same method, solving 73 elementary reactions with 24 reactants [46]. However, the model exhibits numerical instability, and notable calculation errors, ranging from -50% to +100%. The numerical instability and error arises from the ill-conditioning of the Jacobi matrix and the complex iterative algorithms employed to solve large systems of nonlinear partial differential equations. The reaction rate constants are crucial components of the Jacobi matrix, and the significant disparity in their magnitudes results in a high condition number. This, in turn, amplifies the sensitivity of the solution, thereby contributing to the observed instability and calculation errors.

$$\frac{dC_i}{dt} = \delta g_i Q + \sum_p \sum_s k_{ps} C_p C_s - C_i \sum_m k_{im} C_m \quad (1)$$

where δ is conversion factor (=1E-6), g_i is g-value for i-th radiolytic species (mol/kJ), Q is the energy absorption rate(W/m^3), C_i is concentration of i-th species (mol/L), k_{ps} is rate constant of reaction between p-th and s-th species, t is time (s).

To mitigate the numerical instability and calculation errors in the prediction model of nitrogen radiolytic products, it is essential to establish a system with a less ill-conditioned Jacobi matrix and a simplified iterative algorithm. Several approaches can be employed to reduce the condition number of the Jacobi matrix, such as normalizing its component parameters of different orders. Additionally, developing a simpler algorithm can be achieved by reducing the number of equations, which effectively streamlines the computational process. Consequently, this paper proposes a simple model from a point-to-point quasi-stable thermodynamic perspective. By

utilizing the radiation chemical yield (g value) and the equilibrium constant method, a calculation model for nitrogen radiation decomposition products at steady-state equilibrium is established. The model involves the solution of 13 equations, effectively reducing computational complexity and minimizing errors within the range of -25% to +20%. This approach offers a more tractable and efficient means of predicting the composition of nitrogen radiolysis products under equilibrium conditions, while maintaining an acceptable level of accuracy. The simplified model presented in this paper provides a valuable tool for assessing the impact of nitrogen radiolysis on the aqueous chemistry of SMRs, enabling researchers and engineers to make informed decisions regarding the design and operation of these advanced nuclear reactors.

II. NUMERICAL METHOD

A. Radiation system

Radiation can be divided into three parts according to previous researches[31]. At physical stage (about 10^{-15} s), energy transfer occurs and substances will be excited and ionized. At physico-chemical stage ($10^{-15} \sim 10^{-12}$ s), complex processes occur, leading to the formation of transient products including hydrated electron, free radicals and so on. At chemical stage(after 10^{-6} s) diffusion and complex physical process occurs, dynamic equilibrium of transient and unstable products is achieved. The whole process can be sketched as Fig. 1. According to Derek Lister el al. [51], the key parameters in reactor water chemistry include pH, conductivity, and the concentration of oxygen and hydrogen, indicating that stable substances are of more importance than transient ones. Besides, according to the steady-state approximation(SSA), in chain reactions and other continuous reactions, if the intermediate products are very active, have a short life, and do not affect the final state of the reaction the intermediate products can be simplified when calculating the reaction equilibrium, then only the steady-state product reactions with long life can be considered [52–55]. By adopting the quasi-static assumption, the time derivative terms in the system of equations can be simplified. This reduces the complexity of the equations, particularly the time-dependent components, and leads to a more tractable mathematical model. After comprehensively considering the above mentioned factors, the system can be simplified as the reactions of the stable radiolysis substances. Next, the radiation process is simply divided into two parts: primary radiation and subsequent reactions. Primary radiation involves the direct composition of nitrogen and water, yielding primary stable products identified as NH_3, NO, NO_2, H_2 ,O_2 and H_2O_2, as shown in Eqs. 2 and 3. The sketch of the simplification is shown in Fig. 1(a).

$$N_2(g) + H_2O(l) \xrightarrow{\gamma} NH_3(g) + NO(g) + NO_2(g) \quad (2)$$

$$H_2O(l) \xrightarrow{\gamma} H_2(g) + O_2(g) + H_2O_2(l) \quad (3)$$

The quantification of primary radiolytic product yield is conducted through the utilization of the radiation chemical yield, denoted as the g-value,which is defined as the quantity of particles undergoing chemical reactions or being generated when 100 electronvolts (eV) of radiation energy is absorbed by the irradiated medium, as elucidated in Eq. 4.

$$g = \frac{N}{D} \times 100 \quad (4)$$

where N is the number of particles broken down/formed per unit volume of matter, D is radiation dose(eV/cm^3).

The subsequent reactions are listed as TABLE 1. The g-values used in this model, which are based on the original data from Reference [49] and derived from the atom conservation law, are detailed in the supplementary materials. The total decomposition g-value of nitrogen at room temperature is reported to be 9.6 [46]. In PWRs, hydrogen are usually injected into the primary system and which concentration are in the range of 25-50 cc/kg to suppress the radiolytic oxidation of water[56]. Besides, the experiments Ibe conducted are all hydrogen enriched. Consequently, the hydrogen-enriched water environment leads to a higher yield of nitrogen-hydrogen compounds compared to nitrogen-oxygen compounds. Therefore, if in a hydrogen enriched environment, this study posits that the production of ammonia is predominant , with the molar ratio of ammonia (NH_3) to nitric oxide (NO) and nitrogen dioxide (NO_2) being 8:1:1, which means the g-value of ammonia, nitric oxide and nitrogen dioxide at room temperature is 7.68, 0.96 and 0.96. While in a water environment where hydrogen and oxygen levels are comparable, the molar ratio is set as 2:1:1, the g-value of ammonia, nitric oxide and nitrogen dioxide at room temperature is 4.8, 2.4 and 2.4.

However, to the best of our knowledge, there is a paucity of specific data correlating the yield of nitrogen compounds with temperature. It is impropriate to directly employ the value of 9.6 at random temperature in the calculation model. In the previous studies on radiolytic aqueous systems, g-value of temperature has a nearly linear relationship[57]. Besides, the yield of nitrogen increases as temperature increases[46]. So, drawing an analogy, it is hypothesized in this article that the chemical yield of nitrogen compounds increases linearly with temperature elevation, as described by Eq. 5.

$$g = g_{288K} + k(T - 288) \quad (5)$$

where k represents the undetermined coefficient which is a positive value and will be elaborated in the subsequent section , and g_{288K} is the radiolytic chemical yield of nitrogen compounds at 288 K, which value is 9.6.

B. Equilibrium constant method

The radiation process has been streamlined into a multi-component chemical equilibrium problem which can be settled by the Gibbs free energy minimization method or equilibrium constant method. The Gibbs free energy minimization

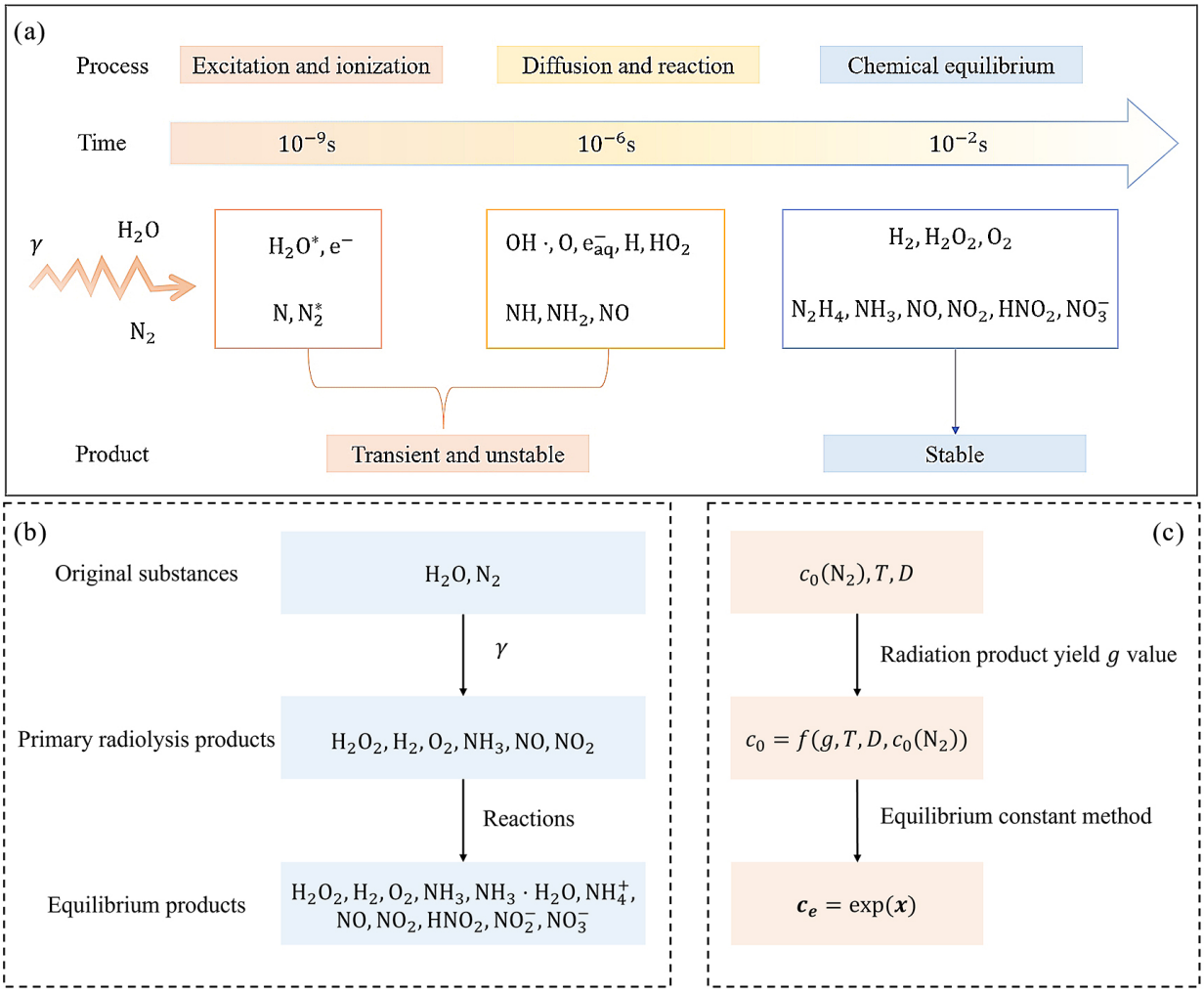

Fig. 1. Scheme of water radioysis and the basic calculation model: (a)scheme of the sequential stages of water radiolysis and the corresponding products; (b)sketch of the simplified substances in the chain reactions; (c) the mathematical expression of the calculation process.

TABLE 1. Reactions adopted in the model

No.	Reaction
1	$H_2O(l) \rightleftharpoons H^+(aq) + OH^-(aq)$
2	$2\,H_2O_2(aq) \rightleftharpoons 2\,H_2O(l) + O_2(g)$
3	$NH_3(g) + H_2O(l) \rightleftharpoons NH_4OH(aq)$
4	$NH_4OH(aq) \rightleftharpoons NH_4^+(aq) + OH^-(aq)$
5	$2\,NO(g) + O_2(g) \rightleftharpoons 2\,NO_2(g)$
6	$2\,NO_2(g) + H_2O(l) \rightleftharpoons HNO_2(aq) + H^+(aq) + NO_3^-(aq)$
7	$HNO_2(aq) \rightleftharpoons H^+(aq) + NO_2^-(aq)$
8	$2\,NO_2^-(aq) + O_2(g) \rightleftharpoons 2\,NO_3^-(aq)$
9	$2\,H_2(g) + O_2(g) \rightleftharpoons 2\,H_2O(l)$
10	$2\,NH_3(g) + 3\,O_2(g) \rightleftharpoons 2\,HNO_2(aq) + 2\,H_2O(l)$

method requires solving a nonlinear programming problem with multiple variables and complex constraints, but it has a slow convergence rate and high initial value requirements . For non-ideal systems, the Gibbs free energy minimization method involves the calculation of fugacity and fugacity coefficients, which is a non-convex problem with a large number of local optimal solutions[58]. On the contrary, the equilibrium constant method exhibits faster convergence and is less stringent with respect to initial values , but it requires prior knowledge of the system's components, the phase states, and the specific reactions[58]. So it is not suitable for complex systems where the phase states and reactions are unknown. As the system state and reactions are known, the equilibrium constant method is a better choice and is employed in this model. The equilibrium constant is defined as the ratio of the concentration product of the reaction products to the concentration product of the reactants when the reaction reaches equilibrium at certain temperature. And the equilibrium constant of Reaction No.1 in TABLE 1 can be written as:

$$K_1 = \frac{[H^+][OH^-]}{[H_2O]} \tag{6}$$

where $[H^+]$ is the concentration of H^+(mol/L), $[H_2O]$ is regulated to be 1 mol/L. According to Van't Hoff equation and Gibbs-Helmholtz expression, the equilibrium constant at any given temperature can also be calculated through the Gibbs

free energy, as delineated in Eq. 7.

$$\Delta_r G_m^{\ominus} = -RT \ln K^{\ominus} \tag{7}$$

Where $\Delta_r G_m^{\ominus}$ is the standard Gibbs free energy of reaction, which can be calculated with Eq. 8, R is molar gas constant which value is 8.314(J/mol·K), T is temperature(K), and $K^{\ominus}$ is the standard equilibrium constant.

$$\Delta_r G_m^{\ominus} = \sum_B v_B \Delta_f G_m^{\ominus}(B) \tag{8}$$

where v_B is the stoichiometric number of substance B in the reaction formula, and it is stipulated that the product is a positive value and the reactant is a negative value. $\Delta_f G_m^{\ominus}(B)$ is the standard Gibbs free energy of formation of substance B, which is related to temperature and follows a quadratic function expression, as described by Eq. 9.

$$\Delta_f G_m^{\ominus} = b + cT + dT^2 \tag{9}$$

The standard Gibbs free energy of formation can be referred to CRC handbook [59] and NIST database [60], and the undetermined coefficients b, c and d are fitted by the least squares method, which are listed in the supplementary materials.

Substance concentrations are concerned quantities, represented as $\boldsymbol{x}$ column vector, where $\boldsymbol{x}(1)$ to $\boldsymbol{x}(13)$ represent [H^+], [OH^-], [O_2], [H_2O_2], [NH_3], [NH_4OH], [NH_4^+], [NO], [NO_2], [HNO_2], [NO_2^-], [NO_3^-], [H_2],respectively.

Therefore, 10 equations of equilibrium constant and quantities to be solved can be established as Eqs. 10 to 19 . Besides, based on atom conservation and charge conservation laws for a closed system, i.e. the initial amount of a specific atom equals the final amount and the solution always maintains electrical neutrality , three more equations can be written as Eqs. 20 to 22.

$$K_1 = \boldsymbol{x}(1)\boldsymbol{x}(2) \tag{10}$$

$$K_2 = \frac{\boldsymbol{x}(4)}{\boldsymbol{x}(3)^2} \tag{11}$$

$$K_3 = \frac{\boldsymbol{x}(6)}{\boldsymbol{x}(5)} \tag{12}$$

$$K_4 = \frac{\boldsymbol{x}(7)\boldsymbol{x}(2)}{\boldsymbol{x}(6)} \tag{13}$$

$$K_5 = \frac{\boldsymbol{x}(9)^2}{\boldsymbol{x}(4)\boldsymbol{x}(8)^2} \tag{14}$$

$$K_6 = \frac{\boldsymbol{x}(10)\boldsymbol{x}(12)\boldsymbol{x}(1)}{\boldsymbol{x}(9)^2} \tag{15}$$

$$K_7 = \frac{\boldsymbol{x}(11)\boldsymbol{x}(1)}{\boldsymbol{x}(10)} \tag{16}$$

$$K_8 = \frac{\boldsymbol{x}(12)^2}{\boldsymbol{x}(11)^2\boldsymbol{x}(4)} \tag{17}$$

$$K_9 = \frac{1}{\boldsymbol{x}(4)\boldsymbol{x}(13)^2} \tag{18}$$

$$K_{10} = \frac{\boldsymbol{x}(10)^2}{\boldsymbol{x}(4)^3\boldsymbol{x}(5)^2} \tag{19}$$

$$\sum_{i=5}^{i=12} \boldsymbol{x}(i) = \boldsymbol{c_0}(5) + \boldsymbol{c_0}(8) + \boldsymbol{c_0}(9) \tag{20}$$

$$\boldsymbol{x}(1) - \boldsymbol{x}(2) + \boldsymbol{x}(7) - \boldsymbol{x}(11) - \boldsymbol{x}(12) = 0 \tag{21}$$

$$\boldsymbol{A}\left(\boldsymbol{x}_{3:13} - \boldsymbol{c}_{0_{3:13}}\right) = 0 \tag{22}$$

$$\boldsymbol{A} = [2, 4, -7, -7, -7, -2, 0, -1, -1, 1, -2] \tag{23}$$

where $\boldsymbol{c}_0$ is the initial concentration column vector containing 13 elements, which elements from the 1st to the 13th correspond to the substances that are consistent with vector $\boldsymbol{x}$.

C. Calculation strategy and boundary conditions

The overall calculation procedure could be described as Fig. 1(b), and the corresponding mathematical expression can be described as Fig. 1(c). The 6 primary radiolytic products, influenced by specified boundary conditions such as temperature, pressure, and radiation dose, engage in mutual reactions along the defined reaction paths (see TABLE 1). This intricate process ultimately achieves chemical equilibrium. Through the equilibrium constant method,the concentrations of the various components involved in the system can be ascertained. Therefore, by the initial nitrogen concentration, temperature dose rate and the radiation chemical yield, the concentration of primary radiolytic products are attained. And by solving the above established Eqs.10 to 23 , the ultimate equilibrium concentrations can be derived.

In this method, the primary challenge lies in solving the set of 13 non-linear equations, and direct resolution proves to be arduous. To mitigate the nonlinear complexity, logarithmic transformations are applied. Additionally, normalization and amplification techniques are employed to diminish numerical errors. The specific methodology is elucidated through Eqs. 24 and 25 and the deformed equations can be referred in the supplementary materials.

$$\boldsymbol{x}' = \ln(r\boldsymbol{x}) \tag{24}$$

$$r = \frac{rand}{|\boldsymbol{x}|_1} \tag{25}$$

where $\boldsymbol{x}'$ is the transformed quantity, r is an amplification coefficient ,*rand* is a random number generated by the computer, $|\boldsymbol{x}|_1$ is the L1 norm of $\boldsymbol{x}$.

Considering a zero-dimensional transient close system, the total irradiation time is divided into N discrete nodes with time step Δt. As Δt is in the order of 1 s, far larger than the equilibrium time scale (1 μs), so it is appropriate to assume that the system attains equilibrium at each time node. Besides, the nitrogen concentration in the system gradually decreases with irradiation, which can be expressed as Eq. 26 while there is no external nitrogen replenishment. And the initial conditions at i-th node are expressed as Eqs. 26 to 29.

$$c_0^{t_{i+1}}(\mathrm{N_2}) = c_e^{t_i}(\mathrm{N_2}) - 1.4\Delta t Q \rho c_e^{t_i}(\mathrm{N_2}) \sum_{\mathrm{X}} (g(\mathrm{X}))/\widetilde{F} \tag{26}$$

$$c_0^{t_{i+1}}(\mathrm{X}) = c_e^{t_i}(\mathrm{X}) + 1.4\Delta t Q g(\mathrm{X}) \rho c_e^{t_i}(\mathrm{N_2})/\widetilde{F} \tag{27}$$

$$c_0^{t_{i+1}}(\mathrm{Y}) = c_e^{t_i}(\mathrm{Y}) + \Delta t Q g(\mathrm{Y}) \rho/\widetilde{F} \tag{28}$$

$$c_0^{t_{i+1}}(\mathrm{Z}) = c_e^{t_i}(\mathrm{Z}) \tag{29}$$

where X represents the primary radiolytic products of nitrogen, including NH_3, NO and NO_2, Y represents the primary radiolytic products of water, including H_2O_2, H_2 and O_2. $c_e^{t_i}(\mathrm{X})$ is the equilibrium concentration of substance X at i-th time node, $c_0^{t_{i+1}}(\mathrm{X})$ is the initial concentration of X at (i+1)-th time node, S is the concentration of nitrogen(mol/L).

The calculation strategy is depicted in Fig. 2. At start, input the physical conditions such as temperature and essential parameters including g-values of water and nitrogen and Gibbs free energy coefficient. Subsequently, the water density and standard Gibbs free energy of reaction are determined, facilitating the calculation of equilibrium constants. Proceeding to the core of the process, the trust-region algorithm is employed to solve the essential equations iteratively over time until reaching t_{end}, where the step tolerance and function tolerance are set as 1e-30. In the end, output the concentrations matrix and end the calculation process.

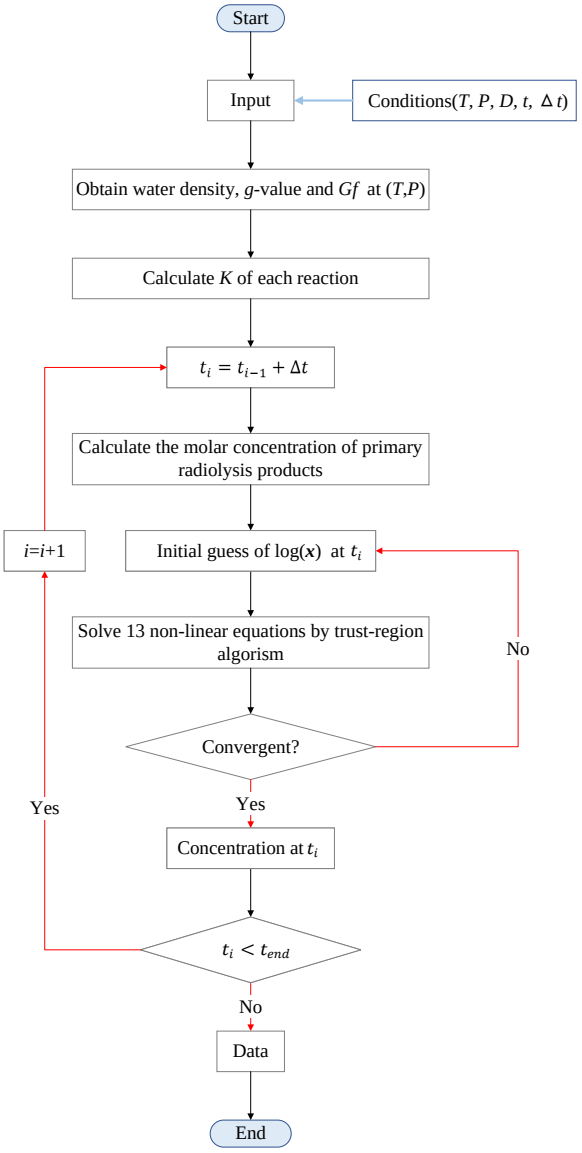

Fig. 2. Calculation strategy

III. RESULTS AND DISCUSSIONS

A. Validation of the model

Experimental data of Ibe et al. is introduced as reference to further assess the accuracy of the calculation model. They conducted gamma irradiation experiments in a pure nitrogen-hydrogen-water environment with temperature ranging from 288 K to 473 K. The experimental conditions are detailed in TABLE 2. They measured the total concentration of dissolved ammonia and ammonium ion, with 20% experimental uncertainty [46]. To test the accuracy of the calculation model, the total ammonia product concentration ($c(\mathrm{NH_3}) + c(\mathrm{NH_4}^+)$) obtained in this paper are compared with both the experimental data and the numerical results from their study. The relative deviation between the numerical results of this paper and the experimental values is introduced as Eq.30. When the coefficient k in Eq.5 is set as 0.1 and Δt set as 1 s, the relative deviation is respectively 5%, 13%,18% and -23% at four temperature cases, as shown in Fig. 4(a), which is within the range of the reported numerical model(-50% to 100%).

$$\delta = \frac{x_{cal} - x_{ref}}{x_{ref}} \times 100\% \tag{30}$$

where δ is relative deviation, x_{ref} is the reference result and x_{cal} is the calculation result.

TABLE 2. Experimental parameters in Ibe's study

T(K)	P(MPa)	c_{N_2}(mol/L)	c_{H_2}(mol/L)	D_γ(Gy/s)
288	9	0.043	0.0215	0.04
373	9	0.03	0.012	0.04
423	9	0.031	0.016	0.04
473	9	0.035	0.024	0.04

B. Discussions of operation parameters

In this model, two important calculation parameters may influence the results: temperature coefficient k in Eq.5 and time step Δt. To comprehensively evaluate the sensitivity of the model to these parameters, a series of sensitivity calculations were performed. The time step Δt was varied within the range of 0.5 to 7, with an increment of 0.1, while the temperature coefficient k was varied between 0 and 0.2, with an increment of 0.01. In total, 1386 parameter combinations were tested.

We observed that the trend of the relative error as a function of Δt remains consistent across different values of k, indicating that the time step is the primary factor affecting the model's performance, regardless of the specific temperature coefficient. Hence, only one representative image illustrating the relationship between Δt and relative error for a fixed value of k is presented in the main text, as shown in Fig.3(a). The absolute value of relative error initially decreases and then increases as Δt increases with temperature ranging from 288 K to 423 K. There are two factor contributing to the trend. From numerical perspective, as the boundary conditions adopted the first-order discretization assumption, the accuracy of the solution improves as the time step Δt decreases. This enhancement occurs because smaller time steps provide a finer temporal resolution, leading to a more precise representation of the continuous dynamics of the system. Specifically, a smaller Δt allows for finer discretization, improving the continuity between discrete points and reducing errors introduced by numerical approximations. However, this gain in accuracy is accompanied by a trade-off in convergence efficiency. Smaller time steps require more iterations to reach a solution, thus increasing the computational cost. Consequently, the balance between accuracy and convergence speed must be carefully evaluated when selecting an appropriate value for Δt . From physical perspective, the reaction requires a certain amount of time to reach a dynamic equilibrium. In the context of this model, as mentioned in section II, we assume a quasi-steady-state condition, meaning that the system is expected to reach equilibrium at each time step. The selection of Δt should be governed by the physical time scales involved in the process, i.e. chemical stage time scale 10^{-6} s. Specifically, the time step must be large enough to ensure that the system has sufficient time to reach equilibrium at each step, but not so large as to violate the assumption of steady-state behavior. Under the point-to-point steady-state assumption, the selection of the time step should align with the actual physical requirement, meaning it should be greater than the equilibrium time. Considering the two factors, it is reasonable to achieve a minimum error at a certain Δt. Furthermore, the error fluctuation does not exceed $\pm 1\%$, indicating the value of Δt has a negligible effect on the results, ensuring the reliability of the model under a wide range of parameter values. Additionally, we observe that across the four temperatures, the optimal value of Δt , which corresponds to the minimum error at each temperature, varies slightly. To determine a general optimal value of Δt for any given temperature, the mean squared relative error (*MSE*) is introduced, which can be calculated by Eq.31. When k is fixed as 0.1, the value of n in Eq.31 is 1. The trend of *MSE* and Δt is shown in Fig.3(b). According to Fig.3(b), the best value of Δt lies between 1.8 and 2.2.

$$MSE = \frac{1}{m}\frac{1}{n}\sum_{i=1}^{m}\sum_{j=1}^{n}\delta_{i,j}^2 \tag{31}$$

where m represents the number of groups (four temperature groups in this paper), n is number of k or Δt groups, δ is the relative error as defined in Eq.30.

Next, the impact of k on the results was evaluated. To quantify this effect, the mean relative error (*MRE*) was calculated using Eq. 32, which assesses the average error across various values of the time step Δt. The relationship of *MRE* and temperature coefficient is depicted in Fig.3(c) . The plot shows that at 288 K, *MRE* stays the same value as k increases. This is because 288 K is the base temperature of temperature coefficient, the results will not be affected by it. At the other three temperatures, the *MRE* initially decreases as k increases, reaching a minimum, and then begins to increase once k surpasses a certain threshold. There exists a minimum error peak at a certain k. However, the k values corresponding to the minimum error vary under the three different temperature conditions. Therefore, to refine the evaluation of k, *MSE* defined in Eq.31 was also calculated. The relationship between *MSE* and k is shown in Fig.3(d). As illustrated, the optimal value of k for minimizing the *MSE* is found to be 0.09.

$$MRE = \frac{1}{n}\sum_{j=1}^{n}|\delta_j| \tag{32}$$

where n is the number of time step, which value is 66 in this paper.

C. Sensitivity analyses of reactor boundary conditions

After determining the optimal operational parameters, the model was employed to calculate the ion concentration and pH value in a certain nuclear reactor equipped with nitrogen pressurizer. To test how the mere nitrogen irradiation phenomena affect the reactor water chemistry, we first considered a posited nitrogen gas pressurized PWR without hydrogen injection or adding any pH regulations, which operating condition is detailed in TABLE 3. In this case, the molar ratio of hydrogen to oxygen produced by water radiolysis is 2:1. Therefore, in the calculation model, the initial g value ratio of NH_3,NO and NO_2 was set to 2:1:1. The equilibrium results,

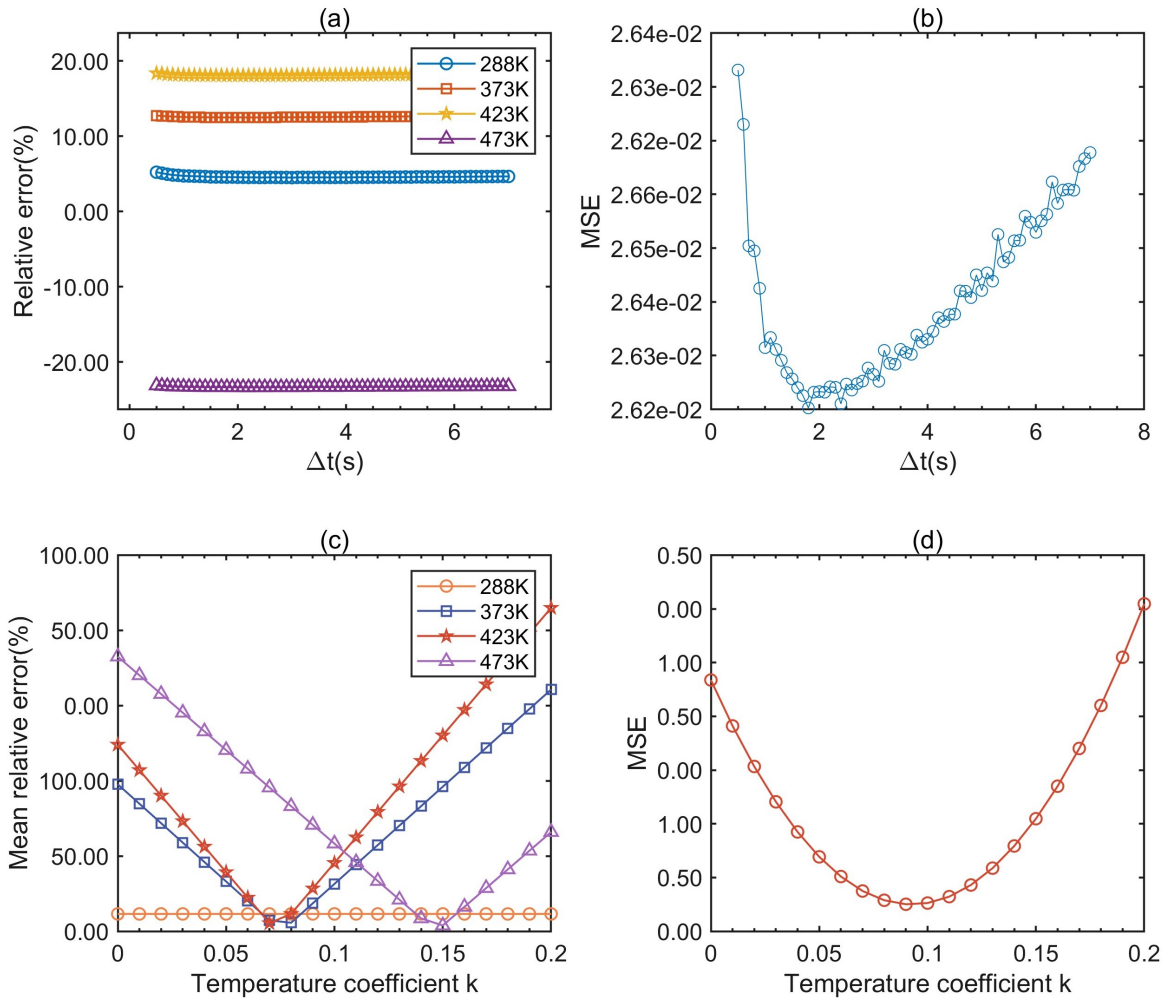

Fig. 3. The results of sensitivity analyses of key parameters: (a)the relationship between relative error and Δt when k is fixed at 0.1 at different temperatures; (b)the relationship between *MSE* and Δt; (c) *MRE* as a function of k at four temperatures; (d)*MSE* as a function of k.

including pH value and concentrations of important ions such as NO_2^-, NO_3^-, and NH_4^+, are depicted in Fig. 4(b) to 4(c). Fig. 4 (b) illustrates that the pH decreases with time (i.e., irradiation dose) and reaches equilibrium in the end, which equilibrium value is 6.8, indicating an alkaline environment. As for ion concentrations, as shown in Fig. 4(c),the concentrations of NO_2^-, NO_3^- and NH_4^+ all increase while time flows and reach equilibrium platform. Besides, the concentration sum of NO_2^- and NO_3^- is smaller than that of NH_4^+. According to the principle of charge conservation, this trend will lead to a large OH^- value and an alkaline water environment, which can interpret the pH line. Moreover, it is noticeable that the NO_2^- concentration is larger than NO_3^-, indicating that the oxygen level is insufficient to fully oxidize the nitrogen oxides generated from the radiolysis of nitrogen at a level of 1000 mg/kg into nitric acid. The similar phenomena was reported in previous study [61]. They reported that in ammonia solution under gamma irradiation, NO_2^- gradually accumulated with time. If the system existed excess oxygen, NO_3^- would generate. Due to the lack of chemical conditions in the primary circuit of real PWRs employing nitrogen pressurizers, direct comparisons between the calculation results and experimental results were not conducted. However, according to Dey et al. [48], with increasing dose, the concentrations of nitrogen-related ions increase slowly to a final stable state. The results in this study are consistent with the aforementioned trends and can be considered reasonable. It is commonly required that the pH at 300 °C in PWRs should be 7.2[62], so the results indicate that in actual nitrogen pressurized PWRs, more ammonia or other alkaline substances should be added to maintain a proper operating water environment.

To determine how physical conditions impact the steady-state pH and to find the best operating conditions for a reactor, we conducted sensitivity analyses by varying one parameter at a time while keeping others constant, in accordance with the settings listed in Table 3. We adjusted the gamma dose rate between 500 to 1500 Gy/s, the temperature from 240 to 320 °C, and the dissolved nitrogen concentration from 50 to 1000 mg/kg separately. This approach allowed us

TABLE 3. Parameters of a given reactor employed nitrogen pressurizer

Item	Value
Average temperature of the primary coolant system	529.15 K
Pressure of the primary coolant system	10 MPa
Concentration of dissolved nitrogen	1000 mg/kg
pH regulation	none
Hydrogen injection	none
γ radiation dose rate	1500 Gy/s

to understand the individual effects of each condition on the pH. As revealed by Fig. 4(d) to (f), increased nitrogen concentration, decreased temperature, and increased dose rate all contribute non-linearly to an increase in the pH value, where dose rate has a relative minor contribution. It is intuitive that as nitrogen concentration decreases, the impact of nitrogen radiolysis on water chemistry diminishes, and the degree of pH deviation from neutrality decreases, i.e. the pH value decreases. Regarding the impact of temperature, the effect of elevated temperatures on the system is multifaceted. On the one hand, increasing temperature promotes the primary yield of hydrogen, oxygen and nitrogen compounds, suggesting that the concentration of total radiolytic products would be expected to rise. On the other hand, temperature affects the equilibrium constants of the ten reactions in TABLE 1, making it difficult to draw a definitive conclusion whether the equilibrium shifts towards the forward reaction or the reverse reaction. Consequently, the net effect of temperature on the system's equilibrium is not straightforward and requires analyses of the interplay between these competing factors. Nonetheless, a significant example which obeys the suppressive effect of higher temperature on pH can be cited that an increase in temperature intensifies the propensity for ammonia to volatilize from water, resulting in a reduction of dissolved ammonia concentration and a subsequent lowering of pH. In general, within the temperature range from 240°C to 320°C, there is an observable suppressive effect of higher temperatures on radiation intensity, with a concomitant decrease in pH as temperature rises. At last, the impact of dose rate is also elucidated. Given that the time step was held constant during the calculations, a reduction in dose rate corresponds to a decrease in the total radiation dose, which in turn attenuates the intensity of the irradiation effect. As a result, this leads to a decrease in ammonia concentration and, to a certain extent, a corresponding reduction in pH. This relationship highlights the dose-dependent nature of radiation-induced chemical changes within the system. Nonetheless, the absolute change in pH across the calculation range is minor, with the relative change amounting to less than 0.2%. This minimal fluctuation is attributed to the ample total calculation time, which allows the system to achieve equilibrium, thereby rendering the impact of dose rate relatively insignificant.

Besides, as for realistic PWRs, hydrogen are usually injected to suppress oxidization, therefore we also evaluated the influence of hydrogen on the system. If hydrogen injection was considered and g ratio of the primary yield of NH_3, NO and NO_2 was set as 8:1:1, the equilibrium pH increased to 7.09 with an injection of 50 cc/kg hydrogen at standard temperature and pressure(STP) , and the pH was 7.08 with 20 cc/kg(STP) hydrogen injection. Additionally, if g ratio was 2:1:1, the equilibrium pH was 6.84 with 50 cc/kg(STP) hydrogen injection, and 6.83 with 20 cc/kg hydrogen injection. It is observed that hydrogen injection will increase the equilibrium pH because the tendency to generate ammonia is enhanced. Besides, g ratio of the primary products exerts an influence on the equilibrium pH, with a relative impact of approximately 3%. This ratio can be construed as an indirect indication of hydrogen concentration, where a predominant yield of NH_3 suggests a hydrogen-enriched environment.

To sum up, the findings suggest that temperature, nitrogen concentration and hydrogen effect are the key factors contributing to the equilibrium results. Given that the temperature in PWRs is commonly maintained at a relative high level, it is recommended to implement hydrogen injection and to incorporate alkaline regulation as part of the chemical control strategy.

IV. SUMMARY

In this paper, we have developed a point-to-point quasi-stable thermodynamic calculation model that employs the equilibrium constant method to analyze the concentrations of nitrogen irradiation decomposition products in water over time. This model was validated with experimental data and was employed in a detailed analysis of varying conditions, offering insights into the behavior of nitrogen species within the aqueous phase. The main conclusions are as follows.

1. Ten key reactions were taken into account in the model, equilibrium constant equations and conservation equations consist of the target system. Normalization of equations were performed to reduce condition number of Jacobi matrix. Quasi-steady and point-to-point assumptions were employed to establish a simple iteration algorithm. Model validation was conducted by comparing with the experimental data of Ibe et al.. The relative calculation error of this model and experimental data is within the range of -25% and 20%, which is smaller than that of the existing model between -50% and 100%.

2. There are two key operation parameters in the model, and the sensitivity analyses of the temperature coefficient and time step were conducted. It reveals that the parameter k exerts a significant influence on the results, while the impact of Δt is relatively minor. The optimal value for k is determined to be 0.09, and for Δt is 2.

3. The equilibrium of primary coolant in a posited nitrogen regulated reactor was calculated. It is found that pH value will gradually increase with irradiation and eventually reach the alkaline state, with the concentration of NO_2^- and NO_3^- ion lower than NH_4^+.

4. The influence of different reactor parameters on the equilibrium state was analyzed. Elevated dose rate, ni-

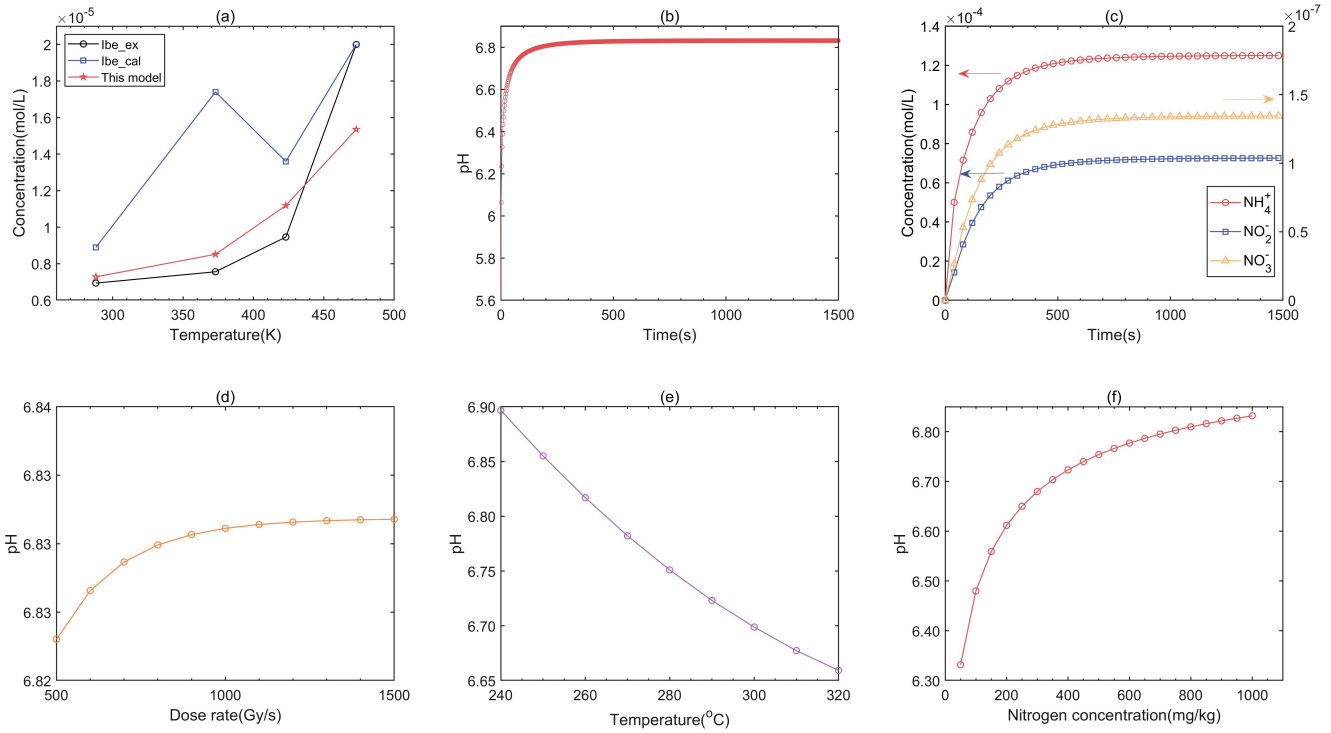

Fig. 4. Validation of the model and the prediction of pH and ion concentration in a certain PWR: (a) the ammonia concentrations of this model, Ibe experimental data and Ibe numerical results; (b) pH change over time in certain PWR; (c)ion concentrations change over time, circle marks represent NH_4^+, square marks represent NO_2^- and triangle marks represent NO_3^-; (d) pH as a function of dose rate; (e)pH as a function of temperature; (f)pH as a function of nitrogen concentration.

trogen concentration and reduced temperature will lead to a higher pH value, which relationships are nonlinear. Dose rate has a minor influence while temperature and nitrogen concentration have notable impact. Additionally, hydrogen injection and the g ratio assignment also has impact on the equilibrium pH. The influence of g ratio assignment of primary yield of NH_3, NO and NO_2 on the result is less than 3%.

5. The results indicate that in nitrogen-pressurized PWRs, temperature, initial material concentration play important roles in the equilibrium pH. It is recommended to implement hydrogen injection and add alkaline regulation to suppress corrosion.

However, there are some deficiencies in this model. For instance, we did not consider multiphase equilibrium and transient flow issues in this model. To more accurately predict the material concentrations distribution in the primary circuit, future considerations should include gas-liquid phase equilibrium and multi-components mass transfer in both one-phase and two-phase flow system.

[1] Y. Sun, Q. Wang, P. Li, et al. Indirect neutron radiography experiment on dummy nuclear fuel rods for pressurized water reactors at cmrr. Nucl. Sci. Tech. **35**, 11, 189 Oct. (2024), doi:10.1007/s41365-024-01534-x.

[2] L. Zhan, Y. Bo, T. Lin, et al. Development and outlook of advanced nuclear energy technology. Energy. Strateg. Rev. **34**, 100630, (2021), doi:10.1016/j.esr.2021.100630.

[3] Q. Wang, J. Guo, R. Li, et al. Exploring the role of nuclear energy in the energy transition: A comparative perspective of the effects of coal, oil, natural gas, renewable energy, and nuclear power on economic growth and carbon emissions. Environ. Res. **221**, 115290, (2023), doi:10.1016/j.envres.2023.115290.

[4] L. Liu, H. Guo, L. Dai, et al. The role of nuclear energy in the carbon neutrality goal. Prog. Nucl. Energy **162**, 104772 (2023), doi:10.1016/j.pnucene.2023.104772.

[5] G. Iyer, N. Hultman, S. Fetter, et al. Implications of small modular reactors for climate change mitigation. Energy Econ. **45**, 144–154 (2014), doi:10.1016/j.eneco.2014.06.023.

[6] X. Yue, M. Y.-P. Peng, M. K. Anser, et al. The role of carbon taxes, clean fuels, and renewable energy in promoting sustainable development: How green is nuclear energy? Renew. Energ. **193**, 167–178 (2022), doi:10.1016/j.renene.2022.05.017.

[7] B. Lin and S. Ullah. Modeling the impacts of changes in

nuclear energy, natural gas, and coal in the environment through the novel dardl approach. Energy **287**, 129572 (2024), doi:10.1016/j.energy.2023.129572.

[8] H. Chen, F. Liu, S. Wang, et al. Accident source term and radiological consequences of a small modular reactor. Nucl. Sci. Tech. **34**, 3, 40 Mar. (2023), doi:10.1007/s41365-023-01192-5.

[9] J. Liou. What are small modular reactors (smrs)? International Atomic Energy Agency, Vienna International Centre, PO Box 100, A-1400 Vienna, Austria, Tech. Rep. First published on 4 November 2021, (2021), https://www.iaea.org/newscenter/news/what-are-small-modular-reactors-smrs.

[10] Z. Liu and J. Fan. Technology readiness assessment of small modular reactor (smr) designs. Prog. Nucl. Energy **70**, 20–28 (2014), doi:10.1016/j.pnucene.2013.07.005.

[11] D. Song. 16 - small modular reactors (smrs): The case of china. in *Handbook of Small Modular Nuclear Reactors (Second Edition)*, second edition ed., ser. Woodhead Publishing Series in Energy, D. T. Ingersoll and M. D. Carelli, Eds. Woodhead Publishing, 2021, 395–408 doi:10.1016/B978-0-12-823916-2.00016-3.

[12] Y. Wang, W. Chen, L. Zhang, et al. Small modular reactors: An overview of modeling, control, simulation, and applications. IEEE Access **12**, 39 628–39 650 (2024), doi:10.1109/ACCESS.2024.3351220.

[13] I. A. E. Agency. *Advances in SMR Developments 2024: Small Modular Reactors*. International Atomic Energy Agency, 2024, Available online.

[14] Q. Xiong, Y. Shen, G. Dang, et al. Design for acp100 long term cooling flow resistance with random forests and inverse quantification. Ann. Nucl. Energy **180**, 109477 (2023), doi:10.1016/j.anucene.2022.109477.

[15] D. Jian, D. Gaojian, D. Shuhua, et al. Analysis of post-loca long-term core safety characteristics for the small modular reactor acp100. Ann. Nucl. Energy **142**, 107349 (2020), doi:10.1016/j.anucene.2020.107349.

[16] V. V. Petrunin, N. V. Sheshina, S. A. Fateev, et al. Scientific and technical aspects of developing a ritm-200n innovative reactor for snpps. At. Energy **134**, 1, 1–10 (2023), doi:10.1007/s10512-023-01020-4.

[17] D. Ingersoll, Z. Houghton, R. Bromm, et al. Nuscale small modular reactor for co-generation of electricity and water. Desalination **340**, 84–93 (2014), doi:10.1016/j.desal.2014.02.023.

[18] H. H. Abdellatif, P. K. Bhowmik, D. Arcilesi, et al. Evaluating direct vessel injection accident-event progression of ap1000 and key figures of merit to support the design and development of water-cooled small modular reactors. Nucl. Eng. Technol. **56**, 6, 2375–2387 (2024), doi:10.1016/j.net.2024.01.049.

[19] S. Nasiri, G. Ansarifar, and M. Esteki. Design of the carem nuclear reactor core with dual cooled annular fuel and optimizing the thermal-hydraulic, natural circulation, and neutronics parameters. Ann. Nucl. Energy **169**, 108939 (2022), doi:10.1016/j.anucene.2021.108939.

[20] Y. S. Kim, S. W. Bae, S. Cho, et al. Application of direct passive residual heat removal system to the smart reactor. Ann. Nucl. Energy **89**, 56–62 (2016), doi:10.1016/j.anucene.2015.11.025.

[21] K. Stevanka and O. Chvala. Deployment of small modular reactors in the european union. Nuclear Science Technology Open Research **2**, 24, 1 (2024), doi:10.12688/nuclscitechnolopenres.17510.1.

[22] X. Wang, M. Wang, J. Zhang, et al. Study on the water seal formation process in advanced pwr pressurizer using cfd method. Ann. Nucl. Energy **135**, 106949 (2020), doi:10.1016/j.anucene.2019.106949.

[23] X. Ma, H. Jia, and Y. Liu. Research on the steam–gas pressurizer model with relap5 code. Nucl. Sci. Tech. **28**, 5, 58 Mar. (2017), doi:10.1007/s41365-017-0223-x.

[24] T. W. Kim, J. W. Kim, and G. C. Park. Development of nonequilibrium pressurizer model with noncondensable gas. Nucl. Eng. Des. **236**, 4, 375–384 Feb. (2006), doi:10.1016/j.nucengdes.2005.09.003.

[25] D. Zhang, S. Qiu, J. Gou, et al. Study of steady and transient characteristics of new nitrogen-typed pressurizer. Nuclear Power Engineering (in Chinese) **27**, z1, 38–42 (2006), doi:10.3969/j.issn.0258-0926.2006.z1.009.

[26] Y. J. Chung, S. H. Yang, and K. H. Bae. A steam or gas pressurizer effect on the system pressure characteristics for an integral pressurized water reactor. Ann. Nucl. Energy **115**, 249–255 (2018), doi:10.1016/j.anucene.2018.01.036.

[27] X. Yan, Y. Li, H. Luo, et al. Transient Simulation Study of Primary Loop Nitrogen-typed Pressurization System. Nuclear Power Engineering (in Chinese) **43**, 3, 33–37 (2022), doi:10.13832/j.jnpe.2022.03.0033.

[28] S. A. Kabakchi, A. V. Luzakov, D. S. Urtenov, et al. Evaluation of the corrosion state of equipment of the first circuit of transport nuclear reactors using the parameters of water chemistry. Therm. Eng. **66**, 3, 183–188 (2019), doi:10.1134/S0040601519030030.

[29] D. S. Urtenov, Y. B. Vorobyev, V. E. Karnaukhov, et al. Features of the Water-Chemical Mode of the I Circuit and Problems of Equipment Operation in the Reactor Units of Atomic Icebreakers. Therm. Eng. **67**, 8, 567–572 Aug. (2020), doi:10.1134/S0040601520080078.

[30] E. Ibe, H. Karasawa, M. Nagase, et al. Chemistry of radioactive nitrogen in bwr primary system. J. Nucl. Sci. Technol. **26**, 9, 844–851 (1989), doi:10.1080/18811248.1989.9734395.

[31] S. Le Caër. Water radiolysis: Influence of oxide surfaces on H_2 production under ionizing radiation. Water **3**, 1, 235–253 (2011), doi:10.3390/w3010235.

[32] M. T. Dmitriev. Doses of ionizing radiation affecting the composition of the atmosphere at radiation laboratories. Sov. Atom Energy **16**, 3, 341–343 (1964), doi:10.1007/BF01122992.

[33] Y. Etoh, H. Karasawa, E. Ibe, et al. Radiolysis of N_2-H_2O systems. J. Nucl. Sci. Technol. **24**, 8, 672–674 (1987), doi:10.1080/18811248.1987.9735864.

[34] V. A. Grachev and A. B. Sazonov. Radiolysis of aqueous ammonia solutions: Mathematical modeling. High Energy Chem. **55**, 6, 472–481 (2021), doi:10.1134/S0018143921060072.

[35] A. R. Jones. Radiation-induced reactions in the N_2-H_2-H_2O system. Radiat. Res. **10**, 6, 655–663 (1959), doi:10.2307/3570649.

[36] Y. J. Kim, G. D. Song, S. H. Baek, et al. Radiochemical behavior of nitrogen species in high temperature water. Nucl. Eng. Technol. (2023), doi:10.1016/j.net.2023.05.020.

[37] M. Wang, T.-K. Yeh, and C. F. Chu. Predicted impact of power uprate on the water chemistry of kuosheng boiling water reactor. Nucl. Eng. Des. **238**, 10, 2746–2753 (2008), doi:10.1016/j.nucengdes.2008.05.007.

[38] M. Wang and T.-K. Yeh. Impact of power uprate on the water chemistry in the primary coolant circuit of a boiling water reactor operating under a fixed core flow rate. J. Nucl. Sci. Technol. **45**, 8, 802–811 (2008), doi:10.1080/18811248.2008.9711481.

[39] M. Wang, T.-K. Yeh, C. F. Chu, et al. Predicted impact of core flow rate on the corrosion mitigation effec-

tiveness of hydrogen water chemistry for kuosheng boiling water reactor. Nucl. Eng. Des. **239**, 4, 781–789 (2009), doi:10.1016/j.nucengdes.2009.01.016.

[40] M. Wang, T.-K. Yeh, H.-M. Liu, et al. Predicted water chemistry in the primary coolant circuit of a supercritical water reactor. Nucl. Sci. Eng. **174**, 2, 179–187 (2013), doi:10.13182/NSE12-16.

[41] T. Tsai, T. Su, T. Wang, et al. Characterization of crud deposited on fuel rods under hwc environment in kuosheng nuclear power plant. Nucl. Sci. Tech. **27**, 1, 1 (2016), doi:10.1007/s41365-016-0013-x.

[42] L. Yuan, J. Peng, M. Zhai, et al. Influence of gamma-radiation on room-temperature ionic liquid [bmim][pf6] in the presence of nitric acid. Radiat. Phys. Chem. **78**, 7-8, 737–739 (2009), doi:10.1016/j.radphyschem.2009.03.064.

[43] Z. Liu, Z. Fang, L. Wang, et al. Alpha radiolysis of nitric acid aqueous solution irradiated by 238pu source. Nucl. Sci. Tech. **28**, 4, (2017), doi:10.1007/s41365-017-0200-4.

[44] Y. Xie, J. Wang, Q. Sun, et al. Effect of strontium and cesium on corrosion and contamination of 316l stainless steels during spent nuclear fuel reprocessing. Prog. Nucl. Energy **154**, 104453, (2022), doi:10.1016/j.pnucene.2022.104453.

[45] Z. Liu, L. Zhang, W. Chen, et al. Effect of oxidizing ions on the corrosion behavior of sin stainless steel in high-temperature nitric acid solution. Electrochim. Acta **442**, 141917, (2023), doi:10.1016/j.electacta.2023.141917.

[46] E. Ibe, H. Karasawa, M. Nagase, et al. Behavior of nitrogen compounds in radiation field and nuclear reactor systems. J. Nucl. Sci. Technol. **26**, 8, 760–769 (1989), doi:10.1080/18811248.1989.9734380.

[47] H. Karasawa, E. Ibe, S. Uchida, et al. Radiation induced decomposition of nitrogen. Int. J. Radiat. Appl. Instrum. Part C **37**, 193–197 (1991), doi:10.1016/1359-0197(91)90126-M.

[48] G. R. Dey. Nitrogen compounds' formation in aqueous solutions under high ionizing radiation: An overview. Radiat. Phys. Chem. **80**, 3, 394–402 (2011), doi:10.1016/j.radphyschem.2010.10.010.

[49] Z. Fang, X. Cao, L. Tong, et al. An improved method for modelling coolant radiolysis in iter. Fusion Eng. Des. **127**, 91–98 (2018), doi:10.1016/j.fusengdes.2017.12.031.

[50] F. Li, Y. Lin, Z. Lin, et al. Research on calculation of coolant radiolysis products in operating conditions during the shutdown of pwrs. Nuclear Power Engineering(in Chinese) **44**, 3, 202–209 (2023), doi:10.13832/j.jnpe.2023.03.0202.

[51] D. Lister and S. Uchida. Determining water chemistry conditions in nuclear reactor coolants. J. Nucl. Sci. Technol. Apr. (2015), doi:10.1080/00223131.2014.973460.

[52] O. Levenspiel. *Chemical Reaction Engineering*, 3rd ed. John Wiley & Sons, 1999.

[53] R. M. Noyes. Generalized kinetics of chemical change: Some conditions for validity of the steady state approximation. Progress of Theoretical Physics Supplement **64**, 295–306 (1978), doi:10.1143/PTPS.64.295.

[54] J. F. Perez Benito. Some considerations on the fundamentals of chemical kinetics: Steady state, quasi-equilibrium, and transition state theory. J. Chem. Educ. **94**, 9, 1238–1246 (2017), doi:10.1021/acs.jchemed.6b00957.

[55] C. V. Rao and A. P. Arkin. Stochastic chemical kinetics and the quasi-steady-state assumption: Application to the gillespie algorithm. J. Chem. Phys. **118**, 11, 4999–5010 (2003), doi:10.1063/1.1545446.

[56] H. Liu, G. Lei, and H. Huang. Review on synergistic damage effect of irradiation and corrosion on reactor structural alloys. Nucl. Sci. Tech. **35**, 3, 57 May (2024), doi:10.1007/s41365-024-01415-3.

[57] A. J. Elliot, M. P. Chenier, and D. C. Ouellette. Temperature dependence of g values for h2o and d2o irradiated with low linear energy transfer radiation. Journal of the Chemical Society, Faraday Transactions **89**, 8, 1193–1197 (1993), doi:10.1039/FT9938901193.

[58] Q. Wei. Study on the calculation of chemical and phase equilibrium in complex system. Master's thesis, Ocean University of China, Qingdao,China, 6 (2007).

[59] D. R. Lide. *CRC handbook of chemistry and physics*. CRC press, 2004, **85**, 907–934

[60] N. I. S. O. U. Chase M W. *NIST-JANAF thermochemical tables*. Washington, DC: American Chemical Society, 1998, **9**, Online.

[61] Z. Guo, Y. Yang, M. Lin, et al. Study on the steady gamma-radiolysis of ammonia solution. Nuclear Power Engineering(in Chinese) **44**, 3, 217–222 (2023), doi:10.13832/j.jnpe.2023.03.0217.

[62] M. Wang. *Irradiated Assisted Corrosion of Stainless Steel in Light Water Reactors - Focus on Radiolysis and Corrosion Damage*. Palaiseau: Laboratoire des Solides Irradiés, 2013, On line. 15–19